Chemical Physics Impact 9 (2024) 100759

Contents lists available at ScienceDirect

Chemical Physics Impact

journal homepage: www.sciencedirect.com/journal/chemical-physics-impact

Green synthesis of Tacrine modified Schiff bases as anti-Alzheimer Agents: An effective strategy validated through in-silico and in-vitro analysis

Presenjit [a,b], Shubhra Chaturvedi [b], Akanksha [c], Deepika Sharma [d], Ritika Chaudhary [e], Prachi Verma [f], Ankita Singh [g], Kaman Singh [a,*]

[a] Department of Chemistry, Babasaheb Bhimrao Ambedkar University, Lucknow-226025, India
[b] Divison of cyclotron and radiological research, INMAS, DRDO, Timarpur, Delhi-110054, India
[c] Department of Zoology, Swami Shraddhanand College, University of Delhi, 110007, India
[d] Department of Chemistry, Banaras Hindu University, Varanasi-221005, India
[e] Dr. B. R. Ambedkar Center for Biomedical Research, University of Delhi, University Enclave, Delhi-110007, India
[f] Department of Chemistry and NanoScience Centre, University of Jyvaskyla, FI-40014, Finland
[g] Department of Chemistry, University of Delhi, Delhi, 110007, India

ARTICLE INFO

Keywords:
Green chemistry
Schiff base
Antioxidant agent
Cholinesterase inhibitor
In-silico analysis
ADMET predication
In-vitro analysis, Alzheimer's disease

ABSTRACT

A variety of Tacrine-modified Schiff base analogues were developed via solvent free (green) method and structurally elucidated using 1H—NMR, FTIR and UV–Vis analysis. High product yield was obtained from the synthesised molecules, which were produced efficiently at room temperature without the need of a solvent. The developed molecules were subsequently assessed for their potential to inhibit acetylcholinesterase (AChE) and butyrylcholinesterase (BChE). These molecules revealed effective inhibition of AChE and BChE enzymes with IC_{50} values varying from 0.1 ± 0.02 to 0.3 ± 0.03 μM and 0.065 ± 0.01 to 0.3 ± 0.03 μM respectively. Compared to the standard Tacrine which has IC_{50} values of 0.35 ± 0.02 μM for AChE and 0.1 ± 0.01 μM for BChE. Notably, compound 3f showed strong inhibition among others for both the enzymes. The structure–activity relationship of derivatives synthesized were verified and established through molecular docking studies. Theoretical ADME studies also predicted excellent drug-likeness for all the synthesized molecules. Antioxidant activities were also assessed because elevated oxidative stress levels are linked with cognitive loss in Alzheimer's disease (AD). These findings suggest that the lead compound is potentially an effective inhibitor for the therapeutic management of AD.

1. Introduction

Alzheimer's disease (AD), is the leading cause of dementia in aged population. It is an invasive neurological condition. [1-3]. It is characterised by a gradual decline of cognitive abilities like speech, attention, decision-making, and memory in particular due to neuronal degeneration in the brain [4,5]. A permanent cure for AD is difficult since the precise mechanisms underlying the cognitive loss and dysfunction are still poorly understood [6]. Present estimates place the global AD population at about 35 million, but estimates suggest that by 2030, that figure could climb to about 65 million, and by 2050, it could reach 115 million [7]. The importance of developing successful treatments is demonstrated by the above statistics. The clinical characteristics of AD that are most prominent include oxidative stress, degeneration of cholinergic neurons located in the basal forebrain, intracellular neurofibrillary tangles caused by excessive tau protein phosphorylation, and extracellular Beta-amyloids [8,9]. The behavioural, functional, and cognitive symptoms of AD are substantially influenced by impaired cholinergic transmission. Thus, as suggested by the cholinergic theory [10,11], acetylcholine (ACh), which has reduced in the brain, can be increased by cholinesterase inhibitors (ChEIs). At the moment, this theory is the only one that is widely acknowledged to explain the nature of Alzheimer's condition [12,13]. This theory is the basis of the mechanisms of AD treatment [14,15]. To improve functioning of chlorogenic system, receptor agonists or cholinesterase inhibitors (ChEIs) are commonly used [16,17]. To date, the US Food and Drug Administration (FDA) has promoted and permitted various acetylcholinesterase (AChE) inhibitors, including galantamine, rivastigmine, donepezil, and tacrine

* Corresponding author.
E-mail address: Singh.kaman@bbau.ac.in (K. Singh).

https://doi.org/10.1016/j.chphi.2024.100759
Received 22 August 2024; Received in revised form 23 September 2024; Accepted 12 October 2024
Available online 18 October 2024

[18].

Apart from the cholinergic theory, several theories have also been brought up to completely explain the aetiology of Alzheimer's illness. Among them are the hypotheses on oxidative stress, tau, and amyloid formation [19]. The oxidative stress hypothesis states that increasing oxidative stress leads to neuronal deterioration and mortality in AD [20]. An essential treatment approach for AD is preventing oxidative stress, which results in neuronal degeneration and death [21,22]. It is well known that antioxidants lessen oxidative stress [21,22]. As a result, an investigation was conducted on the antioxidant properties of the synthesised molecules for this study.

The human body has two different forms of enzymes related to cholinesterase in brain that are AChE and BChE [23]. AChE, a member of hydrolase group, involved in the degradation of acetylcholine (ACh) (Fig. 1), is a neurotransmitter that is crucial for the function of both the mid and peripheral nervous systems. At cholinergic synapses, this enzymatic activity facilitates the termination of nerve signal transmission. [24]. Inhibitors of AChE prevent its breakdown, thereby increasing its concentration and prolonging nerve conduction time [25]. BChE, mainly found in the brain, liver, plasma, and muscle tissues, also participates in the hydrolysis of ACh. Studies suggest that during degenerative alterations involving ACh breakdown, BChE may have a compensatory function in the brain [26-28]. Mechanism of ACh and AChE pathways in AD progression (Fig. 2).

Primary amines condense with aldehydes or ketones to develop the Schiff bases, commonly referred to as imines. According to published research, these molecules represent an important class of molecules that are primarily used in paints, organic intermediates, and catalysts [29, 30]. Additionally, The (C = N) Schiff base have shown a broad spectrum of biological activities, including anti-inflammatory, antiviral, antibacterial, anti-Alzheimer's, antidiabetic, antimalarial, antifungal, and antipyretic properties. .The structural characteristic of Schiff bases, the imine group, is present in many natural compounds and is essential to their biological functions [31]. As a result, Schiff bases have been the subject of numerous and growing publications in the fields of chemistry, pharmacy and biochemistry.

The well-known AChE inhibitor 9-amino-1,2,3,4-tetrahydroacridine, also known as tacrine, is one of the first cholinesterase inhibitor to receive an FDA approval for the treatment of Alzheimer's disease [32]. Based on the crystal structure developed by X-ray of the tacrine-AChE complex, carbonyl oxygen of His440, a crucial residue in the catalytic triad of the enzyme and the protonated nitrogen of tacrine's acridine ring form a hydrogen bond. [33]. In addition, the aryl ring of Phe330 and the indole ring of Trp84, as well as two aromatic rings of tacrine, exhibit π-π stacking [34]. Some of the commercially available drugs for AD treatment including Tacrine are depicted in (Fig. 3).

The synthesis of different derivatives or hybrid compounds as AChE inhibitors has attracted a lot of attention in recent years. A few examples include the derivatives of piperidine [35], tetrazole [36], quinolines [37], hydroxyquinoline derivatives [38], carbamate derivatives [39], β-lactam analogues, Schiff bases (made from modified aniline derivatives and 2-naphthaldehyde) [40], and coumarin derivatives [41]. Various reported synthetic molecules as cholinesterase inhibitors are mentioned below (Fig. 4).

Researchers have concentrated on creating more strong and selective ligands than unmodified tacrine because of its well-established significance as an inhibitor of cholinesterase in therapeutic management of Alzheimer's condition. Many tacrine derivatives were more active than

Fig. 1. Hydrolysis of acetylcholinesterase.

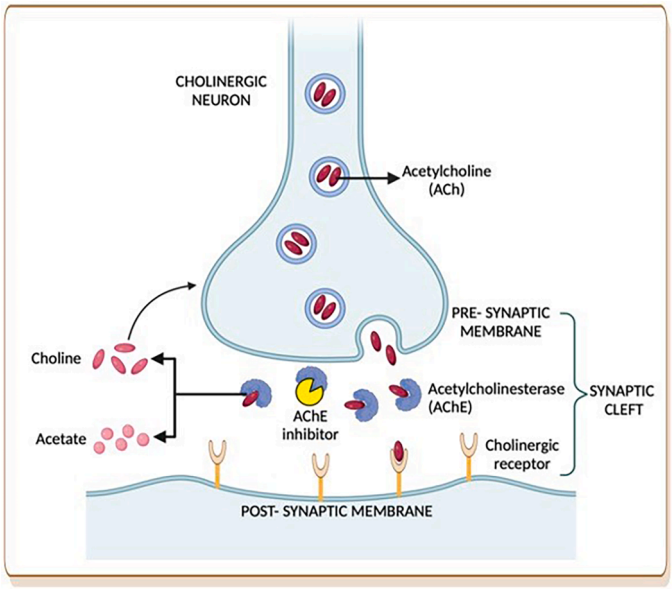

Fig. 2. Cholinergic theory and synaptic pathways in AD progression.

tacrine itself by 2019 after they were synthesised and evaluated for their inhibition progress towards AChE [42]. For example, studies have looked into hybrids like (tacrine-melatonin, ferulic acid, lipoic acid and curcumin) [43-44].

Our study aims to explore the inhibitory efficacy of new Schiff bases against AChE and BChE, In line with the aforementioned outcomes. The tacrine were conjugated with various aromatic aldehyde groups to enhance their inhibitory properties further. Molecular modeling was utilised to propose potential binding affinity of these developed inhibitors within the binding sites of the intended proteins. Additionally, the antioxidant efficacy of the lead molecules were investigated using DPPH assays. To compare the inhibitory and antioxidant effects of the new synthesized Schiff bases, Tacrine was employed as the reference marker.

2. Method and materials

2.1. Instrumentation and chemicals

The chemicals and materials used in the studies were all sourced from Sigma-Aldrich unless specified otherwise. The materials included silica gel (mesh 70–230, particle size 63–200 μm), silica gel 60-coated aluminium TLC plates, 2,2-diphenyl-1-picrylhydrazyl, acetylcholinesterase and butyrylcholinesterase and (Ellman's reagent). BioRender.com was utilised for creating the images. Docking algorithms from the AutoDock Suite were utilised for the interpretation of molecular docking, and BIOVIA Discovery Studio Visualizer was employed for the computational outcome analysis. Tetramethylsilane was employed to represent chemical shifts during the 1H and 13C NMR characterisation that was carried out at the University Science Instrumentation Centre (USIC), Delhi University, using a Jeol JNM-EXCP series 400 MHz FT-NMR. An Orbitrap-based mass spectrometer from Thermo Fischer Scientific was used for high-resolution mass spectrometry (HRMS). ELISA 96 well plate reader (Bio-tek). A VICTOR Nivo multimode microplate reader from Perkin Elmer was used to measure UV absorbance.

2.2. Synthesis of Schiff bases via solvent free (Green) approach

In a mortar and pestle at room temperature, commercially available aldehydes were ground with aromatic amine for twenty to twenty-five minutes without the addition of a solvent or catalyst to create Schiff

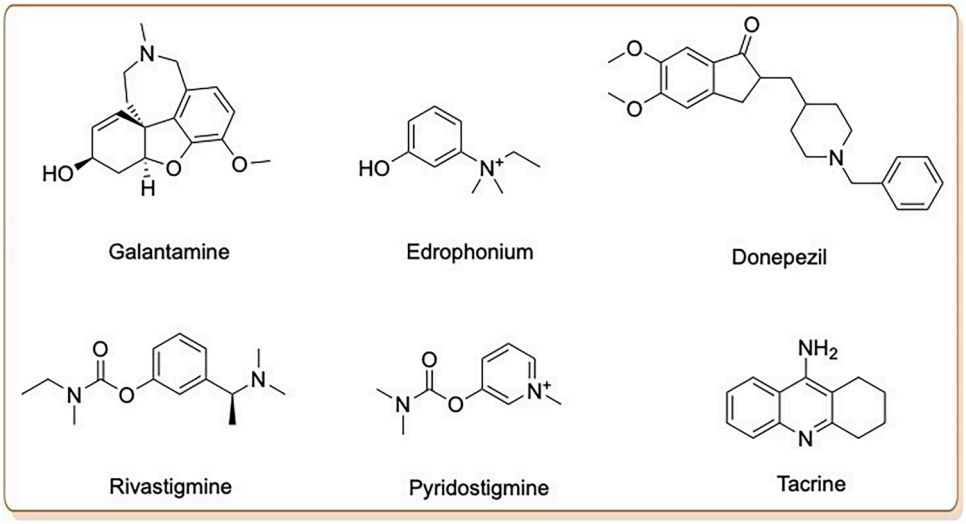

Fig. 3. Examples of pharmaceuticals utilised for Alzheimer's therapy.

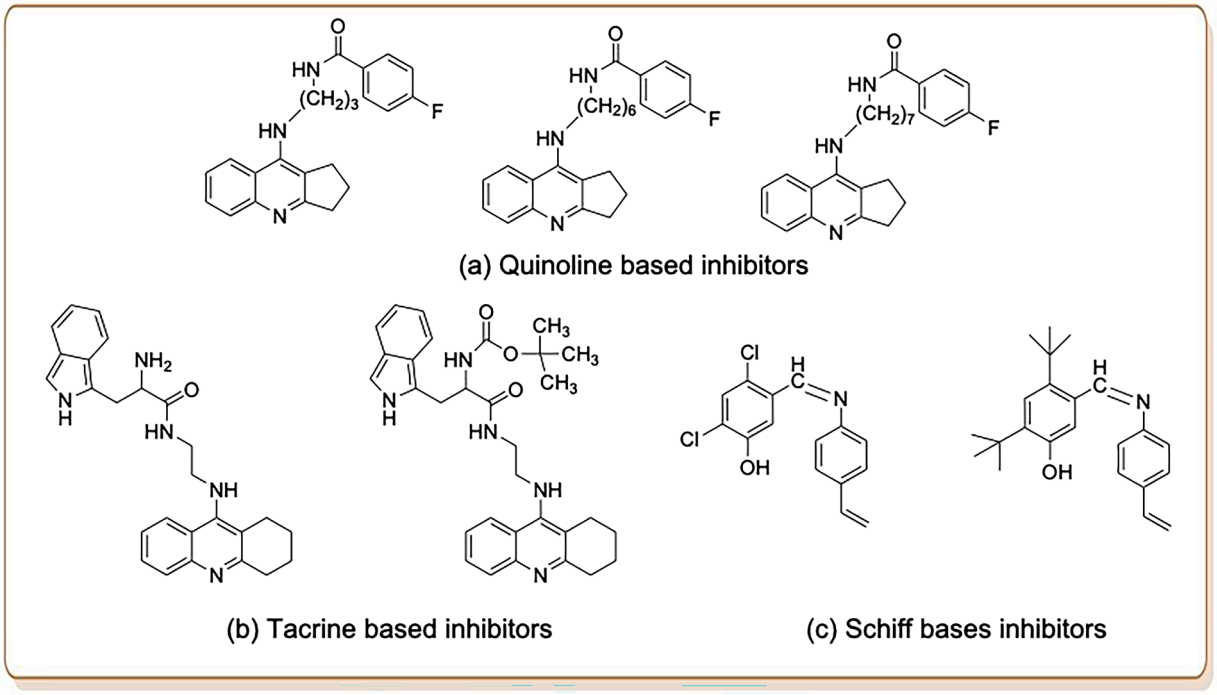

Fig. 4. Some examples of reported cholinesterase inhibitors.

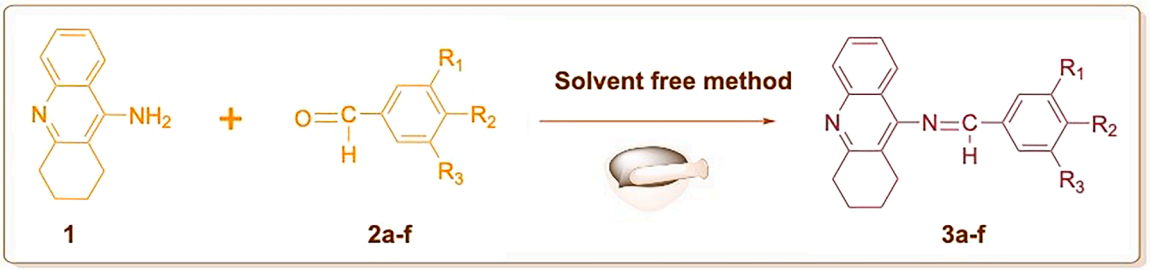

Fig. 5. The green approach synthesis pathway for the development of Tacrine-Schiff bases, **1**: Tacrine, **2a**: 4-methoxybenzaldehyde, **2b**: 3,4-dimethoxybenzaldehyde, **2c**: 3,4,5-trimethoxybenzaldehyde, **2d**: 3-chlorobenzaldehyde, **2e**: 4-(dimethylamino)benzaldehyde, **2f**: indole-2-carbaldehyde. **3a**: R_1═*H*, R_2═OMe, R_3═*H*, **3b**: R_1═*H*, R_2═OMe, R_3═*H*, **3c**: R_1═OMe, R_2═OMe, R_3═OMe, **3d**: R_1═OMe, R_2═OMe, R_3═OMe, **3e**: R_1═*H*, R_2═*N*-Di-OMe, R_3═*H*, **3f**: Indole-2-carbaldehyde.

bases. The reaction progress was analysed through TLC, which produced a paste. The mixture was finished by evaporating the water until it was dry, and the powder that was left over was recrystallised in pure methanol [45]. Spectroscopic methods such as Nuclear Magnetic Resonance, UV–Vis and Infrared Spectroscopy were utilised to characterise the synthesised molecules. The formation of tacrine-Schiff bases synthetic scheme is represented in (Fig. 5).

2.3. Cholinesterase inhibition activity assay

The inhibition progress of the developed molecules on the cholinergic enzymes acetylcholinesterase (AChE) and butyrylcholinesterase (BChE) were examined through Ellman method [46]. A concentration of 0.22 units/mL was used to formulate the enzyme solution. Tacrine and the synthesised molecules were investigated at concentrations ranging from 1.36 to 0.085 μM. Standard tacrine (TAC) and the developed compounds were soluble in methanol. In each well of a 96-well plate, 100 μL of phosphate buffer was added with (pH 6.7). The investigated molecules sample (20 μL) and AChE (20 μL/well) were added in varying quantities to the wells, and were incubated for 10 min at 25 °C. To initiate the reaction, the enzyme-inhibitor mixture was mixed with the substrate, acetylthiocholine iodide (3 mM, 50 μL/well), and 5,5-dithio--bis2-nitrobenzoic acid (3 mM, 50 μL/well). For ten minutes, the yellow anion's formation was monitored at 412 nm. A control was provided with an identical enzyme solution devoid of the compounds. A blank read was used to adjust the control and inhibitor readings. The analysis was conducted three times. A triplicate of the study was conducted. The concentrations of the prepared samples that suppressed the breakdown of the (acetylcholine) by 50 % (IC50) were found, using the linear regression approach between percent inhibition and sample concentration. [47].

2.4. Antioxidant activity via DPPH radical scavenging strategy

Using the 2,2-diphenyl-1-picrylhydrazyl radical scavenging method described in the literature [48], the antioxidant potential was evaluated [48]. To obtain different concentrations, varying volumes of each sample solution were added to a 2.5 mL solution of DPPH (0.002 %) in methanol. Following a half-hour incubation period at room temperature, the absorbance was taken at 516 nm and was calculated in comparison to methanol (blank). The standard formula given below was used to calculate the antioxidant activity:

$$\% \mathbf{AA} = -\mathbf{A}_{\mathrm{DPPH}} - \mathbf{A}_{\mathrm{Sample}} / \mathbf{A}_{\mathrm{DPPH}}$$

The experiment organised and executed in triplicate. The antioxidant activity was plotted against the compound concentration in order to determine the concentration that gave 50 % antioxidant activity (IC_{50}) [48-49].

2.5. Pharmacological features of ligands(ADMET)

The first screening was conducted using SwissADME (http://www.swissadme.ch/) (Absorption, Distribution, Metabolism, and Excretion), an online web-based platform that evaluates the pharmacological accuracy of drug candidates [50]. This tool investigated a number of attributes, such as lipophilicity, molecular weight, and the quantity of donors and acceptors of hydrogen bonds. Potential candidates were assessed for drug-likeness based on six physicochemical features: solubility, molecular size, lipophilicity, polarity, saturation, and flexibility. The Lipinski rule of five is based on these characteristics. As a result, molecules that varied from the threshold values were not included in the analysis that was conducted. Furthermore, the pkCSM and ADMETlab 2.0 website was used to forecast the ligands toxicity.

2.6. Molecular modelling

Molecular docking study was preceded by pre-processing proteins with Discovery Studio Visualizer (v21.1.0.20298) [51]. Any hetero groups were eliminated at this point, and hydrogen atoms and other charges were added. The reported literature and the CASTp server (http://cast.engr.uic.edu) provided the active site residues and coordinates [52]. ChemBioDraw Ultra 14.0 was used to draw the 2D structure. The tool for acquiring the 3D configuration was ChemBio3D Ultra 14.0, which was included in the same package. Additionally, ligands and receptors were prepared in the PDBQT file format using the AutoDock tool (v1.5.6, https://autodock.scripps.edu). To obtain a more comprehensive understanding of the interactions between ligands and receptors, AutoDock Vina (https://vina.scripps.edu) was aided with molecular docking [53]. Finally, a rigid-flexible docking was carried out after the receptor binding sites were encircled in a grid box. Table 1 lists the amino acid present at the active site of the targeted PDB's.

The active site of the protein structure with PDB ID: 4EY6 features crucial amino acid residues that support its enzymatic role, particularly in catalyzing hydrolytic reactions like those of acetylcholinesterase (AChE). His447, Ser203, and Glu202 form a catalytic triad, a common motif in enzymes that drive substrate hydrolysis. Trp86 plays an important part in substrate binding, stabilizing interactions within the active site. Additionally, residues such as Tyr124, Tyr337, Tyr449, and Phe338 contribute to aromatic stacking, which helps stabilize ligands or substrates and ensures the structural cohesion of the protein-ligand complex.

In the case of PDB ID: 4BDS, the active site is composed of various residues that promote enzymatic reactions and substrate attachment. Ser287 and His438 are likely involved in catalytic processes. Aromatic residues like Trp82, Tyr332, Tyr440, Trp231, and Phe398 participate in hydrophobic interactions and stabilize ligands via aromatic stacking. Residues such as Asn68, Gln119, Asp70, Thr120, and Ser198 may engage in hydrogen bonding or interact with the ligand's polar groups, enhancing binding specificity. Hydrophobic residues, including Ile69, Leu286, Val288, and Met437, shape the hydrophobic pocket of the active site, aiding in the attachment of nonpolar portions of the substrate. These active site residues play key roles in binding, hydrolysis, and ligand stabilization, contributing to the overall enzymatic function of the proteins.

3. Result and discussion

3.1. Chemistry

In this work, a number of Schiff bases were created by combining aromatic amines with commercially accessible aldehydes in a mortar and pestle and grinding the mixture for twenty to twenty-five minutes at room temperature without the use of a catalyst or solvent. The resultant paste was recrystallised in methanol after being allowed to dry for a whole night (Fig. 5). All the developed molecules were characterized using NMR, FTIR and UV–Vis and the comprehensive details are

Table 1
The detail of amino acid residues responsible for enzymatic activity at the active site of the targeted protein.

PDB ID:	Active site amino acid residues
4EY6	His447, Trp86, Ser203, Tyr124, Tyr449, Glu202, Tyr337 and Phe338
4BDS	Ser287, Asn68, His438, Ile69, Trp82, Asp70, Gln119, Thr120, Ser198, Trp231, Leu286, Val288, Tyr332, Phe398, Trp430, Met437, Phe329 And Tyr440.

Note: Trp: Tryptophan, Tyr: Tyrosine, Ser: Serine, Glu: Glutamic Acid, Phe: Phenylalanine, His: Histidine, Asn: Asparagine, Ile: Isoleucine, Asp: Aspartic Acid, Gln: Glutamine, Thr: Threonine, Leu: Leucine, Val: Valine, Met: Methionine.

described below. The technical data are provided in (Supplementary file).

3.1.1. Synthesis of compound (**3a**)

The compound was obtained with a notable yield of 84 %, signifying an effective and highly efficient reaction. 1H NMR analysis (400 MHz, DMSO) provided several distinct signals: a doublet at δ 9.87 ppm (J = 8.9 Hz, 1H) likely indicates a proton connected to an imine group. Another doublet at δ 7.92 ppm (J = 8.4 Hz, 1H) falls within the aromatic region, hinting at the presence of a conjugated system. Additional peaks include a quartet at δ 7.84 ppm (J = 10.2 Hz, 1H) and a multiplet between δ 7.62–7.54 ppm (1H), both corresponding to aromatic protons involved in more complex interactions. A doublet at δ 7.25 ppm (J = 10.0 Hz, 2H) represents protons in a para-substituted aromatic ring. Peaks at δ 3.75, 2.97, 2.56–2.50, and 1.83 ppm reflect the presence of methylene, methine, and methyl groups. ^{13}C NMR data confirmed the existence of a C = N bond at δ 153 ppm, a typical feature of Schiff bases. UV–Vis spectroscopy demonstrated a λ_{max} of 320 nm, consistent with π–π* transitions found in conjugated systems. FTIR analysis further validated the structure, identifying characteristic absorption bands at 1653 cm^{-1} (C = N), 2930 cm^{-1} (aromatic C–H), and 2860 cm^{-1} (cycloalkyl C–H), confirming the presence of both aromatic and cycloalkyl structures. This comprehensive analysis affirms the successful synthesis and structural confirmation of the compound.

3.1.2. Synthesis of compound (**3b**)

The compound was synthesized with an 86 % yield. The 1H NMR spectrum (400 MHz, DMSO) revealed a singlet at δ 9.35, attributed to the imine proton (C = N), characteristic of Schiff bases and indicative of a highly deshielded environment. Other notable features included a doublet at δ 8.02 (J = 8.4 Hz) for an aromatic proton, a doublet of doublets at δ 7.39 (J = 24.0, 7.8 Hz) showing intricate coupling of aromatic protons, and a multiplet between δ 7.12 and 7.04 for two additional aromatic protons. Additional doublets at δ 6.89 (J = 1.7 Hz) and δ 6.68 (J = 8.2 Hz) further described aromatic protons with varying coupling constants. Singlets at δ 3.35 and δ 9.35 represented a methyl group and the imine proton, respectively, while multiplets at δ 2.06–2.02 and δ 1.41–1.31 indicated a cycloalkyl or aliphatic chain. The 13C NMR spectrum verified Schiff base formation with a peak at δ 156 ppm, corresponding to the deshielded carbon of the imine group. UV–Vis spectroscopy showed a maximum absorbance at 320 nm, typical for π–π* transitions, confirming a conjugated system. FTIR analysis provided further evidence of the Schiff base structure, with a peak at ν(C = N) = 1657 cm^{-1} for the imine bond, and additional peaks for aromatic (ν(C–H) = 2961 cm^{-1}) and cycloalkyl (ν(C–H) = 2848 cm^{-1}) groups. These results collectively demonstrate the successful formation and structural integrity of the Schiff base compound.

3.1.3. Synthesis of compound (**3c**)

The molecule was synthesized with a yield of 83 %. The 1H NMR spectrum (400 MHz, DMSO) revealed a singlet at δ 9.85 ppm, indicating the deshielded imine proton (C = N), a defining feature of Schiff base compounds. The spectrum also showed a doublet at δ 8.51 ppm (J = 8.5 Hz) and a triplet at δ 7.84 ppm (J = 7.8 Hz), suggesting intricate coupling among the aromatic protons. A singlet at δ 7.55 ppm represented an isolated aromatic proton, while the doublet at δ 7.10 ppm (J = 8.5 Hz) pointed to additional coupling within the aromatic region. Aliphatic protons appeared as singlets at δ 3.84 ppm, 3.16 ppm, and 2.96 ppm, alongside a multiplet from δ 1.86 to 1.77 ppm. In the 13C NMR spectrum, a peak at δ 165 ppm confirmed the presence of the imine carbon (C = N), underscoring the formation of the Schiff base. The UV–Vis analysis revealed a maximum absorbance at 340 nm, consistent with π–π* transitions, which confirmed the conjugation between the imine group and aromatic rings. FTIR spectroscopy further validated the Schiff base structure with a prominent imine stretch at ν 1648 cm^{-1}, in addition to C–H stretching vibrations for aromatic and cycloalkyl groups at ν 2959 cm^{-1} and ν 2831 cm^{-1}, respectively. The spectroscopic data confirmed the successful synthesis and structural validation.

3.1.4. Synthesis of compound (**3d**)

The compound was successfully synthesized, yielding 82 %. The 1H—NMR spectrum exhibited a doublet at δ 8.41 ppm (J = 7.8 Hz), corresponding to the imine proton (C = N), a key indicator of Schiff base formation. Additionally, a broad multiplet between δ 7.13–7.80 ppm was observed, representing the aromatic protons of the tacrine structure. The 13C—NMR spectrum displayed a signal at δ 156 ppm, confirming the imine carbon and further supporting the presence of the Schiff base. FTIR analysis provided additional evidence, showing a distinct C = N stretching band at 1663 cm^{-1}, along with peaks at 2941 cm^{-1} and 2827 cm^{-1}, indicating aromatic and cycloalkyl C—H stretching. UV–Vis spectroscopy revealed a maximum absorbance at 340 nm, attributed to π–π* transitions, demonstrating the extended conjugation between the imine and aromatic rings.

3.1.5. Synthesis of compound (**3e**)

The yield of the developed molecule was 84 %. In the 1H—NMR spectrum, a doublet of doublets at δ 8.53 ppm (J = 8.6, 3.1 Hz) was observed, corresponding to the imine proton (C = N), which is characteristic of Schiff base formation. The aromatic region displayed complex signals, including quartets at δ 7.82 ppm (J = 7.8 Hz) and δ 7.55 ppm (J = 8.1 Hz), as well as multiplets at δ 7.68–7.62 ppm and δ 6.77–6.71 ppm, reflecting coupling interactions within the aromatic system. Aliphatic protons appeared as a doublet at δ 2.96 ppm (J = 5.9 Hz) and a pentet at δ 1.82 ppm (J = 7.6 Hz), indicating methylene and cycloalkyl groups. In the 13C—NMR spectrum, the imine carbon resonated at δ 156 ppm, confirming Schiff base formation. FTIR analysis further supported this, showing a distinct C = N stretching vibration at 1646 cm^{-1}, alongside C–H stretching vibrations at 2947 cm^{-1} and 2821 cm^{-1} for the aromatic and cycloalkyl components, respectively. The UV–Vis spectrum revealed a maximum absorbance at 330 nm, indicative of π–π* transitions, which reflects the conjugated system between the imine group and the aromatic rings. These findings confirm the key role of the imine bond and aromatic framework in the molecule.

3.1.6. Synthesis of compound (**3f**)

A Schiff base derivative was synthesized with an 88 % yield. The 1H—NMR spectrum revealed various signals that shed light on the molecule's structure. A doublet at δ 13.84 ppm (J = 3.4 Hz) indicated a proton from a phenolic -OH group, which is highly deshielded due to hydrogen bonding. The multiplet at δ 12.49–12.45 ppm likely corresponds to an amine or NH group, exhibiting broadening from proton exchange effects. Singlets observed at δ 9.91 ppm and δ 8.90 ppm were assigned to protons from an aldehyde or aromatic ring and another aromatic system, respectively. The aromatic protons displayed diverse coupling patterns: a doublet at δ 8.48 ppm (J = 8.5 Hz) and doublets at δ 8.27 ppm (J = 3.4 Hz) and δ 8.06 ppm (J = 7.8 Hz) indicated different interactions within the aromatic region. Additional aromatic protons appeared as triplets and doublets of triplets between δ 7.73 ppm and δ 7.17 ppm, reflecting complex coupling. A singlet at δ 3.78 ppm was attributed to a methoxy group, while triplets at δ 2.88 ppm (J = 5.9 Hz) and δ 2.43 ppm (J = 6.1 Hz) represented aliphatic protons. A multiplet at δ 1.78–1.68 ppm was associated with protons in flexible chain segments. The ^{13}C—NMR spectrum showed a peak at δ 150 ppm, confirming the presence of the imine group integral to the Schiff base. FTIR analysis revealed a strong band at 1651 cm^{-1}, confirming the imine bond, along with C–H stretching vibrations at 2939 cm^{-1} and 2832 cm^{-1}, indicating the presence of aromatic and cycloalkyl groups. UV–Vis spectroscopy showed a peak at 330 nm, characteristic of π–π* transitions, which supports the presence of a conjugated system.

3.2. Biological analysis

3.2.1. AChE/BChE inhibition analysis

AChE and BChE were examined as targets for the *in-vitro* analysis of Schiff base derivatives (3a-f). All Schiff base compounds modified with tacrine, as indicated in Table 2, strongly reduced AChE (IC_{50} values: 0.1 ± 0.02 to 0.3 ± 0.03 μM) and BChE (IC_{50} values: 0.065 ± 0.01 to 0.3 ± 0.03 μM). For AChE and BChE, the IC_{50} values of tacrine (a standard inhibitor), were 0.35 ± 0.02 μM and 0.1 ± 0.01 μM respectively. Among the derivatives, molecule 3f demonstrated the maximum inhibition activity, with IC_{50} values of 0.1 ± 0.02 μM for AChE and 0.065 ± 0.01 μM for BChE. Moreover, the other synthesized Schiff base molecules also effectively inhibited the target enzymes, showing greater inhibitory potency than the standard inhibitor Tacrine. The Selectivity Index (SI) ratio is utilized in inhibition studies to assess how selectively a compound inhibits one enzyme compared to another. This ratio helps optimize enzyme inhibition by ensuring that the drug targets the desired enzyme efficiently and appropriately, aligning with specific therapeutic requirements. The statistical data of the Schiff base analogues are represented in (Fig. 6).

3.2.2. Antioxidant efficacy via DPPH radical scavenging strategy

In AD, over-production of reactive oxygen species (ROS) responsible for oxidative stress, leading to neuronal damage. Antioxidants help neutralize ROS, reduce oxidative stress, and protect neurons, making them potential therapeutic agents for the disease. Antioxidants scavenge free radicals, chelate metal ions, and increase the activity of endogenous antioxidant enzymes to protect neuronal cells from damage and possibly minimize the progression of AD. The 2,2-diphenyl-1-picrylhydrazyl radical scavenging activity, which has been described earlier, was used to evaluate the antioxidant activity. The DPPH radical scavenging assay reveals that the antioxidant activity of the derivatives varied between 354 ± 4 μM and 763 ± 6 μM. The molecule that showed the maximum antioxidant activity among all the synthesised ligands was compound 3f, which is a Schiff base molecule based on indole-2-carbaldehyde (IC_{50} = 354 ± 4 μM). Furthermore, the other compounds demonstrated enhanced antioxidant activity, with improvements ranging from one to four times, when compared to the reference compound, tacrine (IC_{50} = >1000 μM). Table 3 displayed the antioxidant activity values for each Schiff base derivative.

3.3. Structure activity relationship (SAR) for AChE and BChE inhibition studies

The synthesised Schiff base scaffolds (3a-e) were split into three sections in order to ascertain and streamline the structure-activity relationship (SAR) for BChE and AChE inhibition studies: Schiff base, tacrine, and substituents R1, R2, and R3. These substituents may be groups that donate electrons or withdraw electrons. Compound 3f is composed of indole-2-carbaldehyde, which belongs to the heterocyclic group (Fig. 7).

Among the synthesized molecules (3a-f), compound 3f demonstrated the maximum inhibition against both enzymes, exhibited IC_{50} values of 0.1 ± 0.02 μM and 0.065 ± 0.01 μM for AChE and BChE respectively, compared to Tacrine's IC_{50} values. This enhanced activity may be because of the presence of heterocyclic moiety indole-2-carbaldehyde attached to the Schiff base. Compounds 3a, 3b, and 3c showed IC_{50} values of 0.15 ± 0.02, 0.3 ± 0.03, and 0.17 ± 0.01 μM respectively for AChE. For BChE, these compounds were less effective compared to AChE, with IC_{50} values of 0.12 ± 0.01, 0.08 ± 0.01, and 0.1 ± 0.01 μM, respectively. However, they still demonstrated increased inhibitory activity compared to Tacrine, likely due to the presence of an OMe group at R_2 in 3a, and groups at R_1 and R_2 in 3b, and at R_1, R_2, and R_3 in 3c. Compound 3d had 0.21 ± 0.01 μM and 0.07 ± 0.01 μM IC_{50} values for AChE and BChE respectively, showing better inhibition for both enzymes compared to Tacrine. This compound has a chloro (Cl) group at the R_2 position. Compound 3e exhibited IC_{50} values of 0.24 ± 0.02 μM for AChE and 0.08 ± 0.009 μM for BChE, also outperforming Tacrine, with a dimethylamino group at the R_2 position.

Based on the SAR analysis, Tacrine-modified Schiff base derivatives carrying a heterocyclic group substituted by benzaldehyde showed promising inhibitory potential. Changes in the substituents at the R_1, R_2, and R_3 positions also influenced the variations in inhibitory activity. To further support these outcomes, a docking study was carried out on compound 3f, that provided insights into the complex interaction among the synthesized molecule and enzymes' active site.

Table 2
IC50 values (μM) of the synthesized compounds for AChE and BChE.

Compound	AChE, IC_{50} (μM)[a]	BChE, IC_{50} (μM)[a]	Selectivity Index[b]
3a	0.15 ± 0.02	0.12 ± 0.01	0.8
3b	0.3 ± 0.03	0.08 ± 0.01	0.26
3c	0.17 ± 0.01	0.1 ± 0.01	0.58
3d	0.21 ± 0.01	0.07 ± 0.01	0.7
3e	0.24 ± 0.02	0.08 ± 0.009	0.27
3f	0.1 ± 0.02	0.0065± 0.01	0.065
Tac	0.35 ± 0.02	0.1 ± 0.01	0.28

[a] IC_{50} are provided according to three parallel results.
[b] Selectivity Index = IC_{50} (BChE)/ IC_{50} (AChE).

3.4. In-silico analysis

Several software tools, such as AutoDock (version 1.5.6) and Discovery Studio Visualizer (DSV), were used to perform docking studies on the strongest analogue in order to visualise 2D and 3D molecular structures within the protein complex. Using the most effective scaffold against AChE and BChE, we conducted docking analyses in order to demonstrate the significant connection between in vitro and in silico research [54-56]. The purpose was to elucidate the interaction between the active scaffold (compound 3f) and the enzymes' active site, which are crucial for their function. These outcomes were further supported by examining protein-ligand interactions, as detailed in Table 4. Notably, the results emphasize the importance of these scaffold molecules in enhancing the enzymatic activities of AChE and BChE.

For AChE enzyme, compound 3f, the most active ligand among the identified lead compounds, demonstrated significant interactions with the active site amino acid residues (PDB: 4EY6) and achieved docking score of −11.3 kcal/mol, outperforming Galantamine (reference compound), which had −9.5 kcal/mol binding affinity score. Figs. 8 and 9 shows the docking conformations of the chosen ligand. In the ligand, the nitrogen in the indole ring created hydrogen bond with the TYR124 residue, while carbon of the Schiff base formed hydrogen bonds with TYR337, within the catalytic active site (CAS). The presence of these hydrogen bonds enhances both the binding capability and the degree of inhibition. The ligand also exhibited Vander Waal interactions with SER203 and HIS447 of the catalytic triad, along with several other significant interactions. For BChE, the ligand exhibited significant interactions with the active site residues of the enzyme (PDB: 4BDS), and achieved docking score of −10.8 kcal/mol, surpassing reference compound Tacrine (−8.2 kcal/mol binding affinity score). The nitrogen on the aromatic ring of the tacrine in the Schiff base molecule formed a hydrogen bond with TRP82, and the same ring was engaged in a pi-anion interaction with ASP70. Within the active site, the indole moiety of the ligand developed π-π stacked, amide π-stacked, and π-alkyl interactions with TRP231, PHE329, and GLY116 residues. Additionally, ligand demonstrated Vander Waal interactions with SER198 and HIS438 of the catalytic triad, along with several other significant interactions. These interactions are crucial for the enzymatic activity of AChE and BChE exhibited by the lead Schiff base molecule.

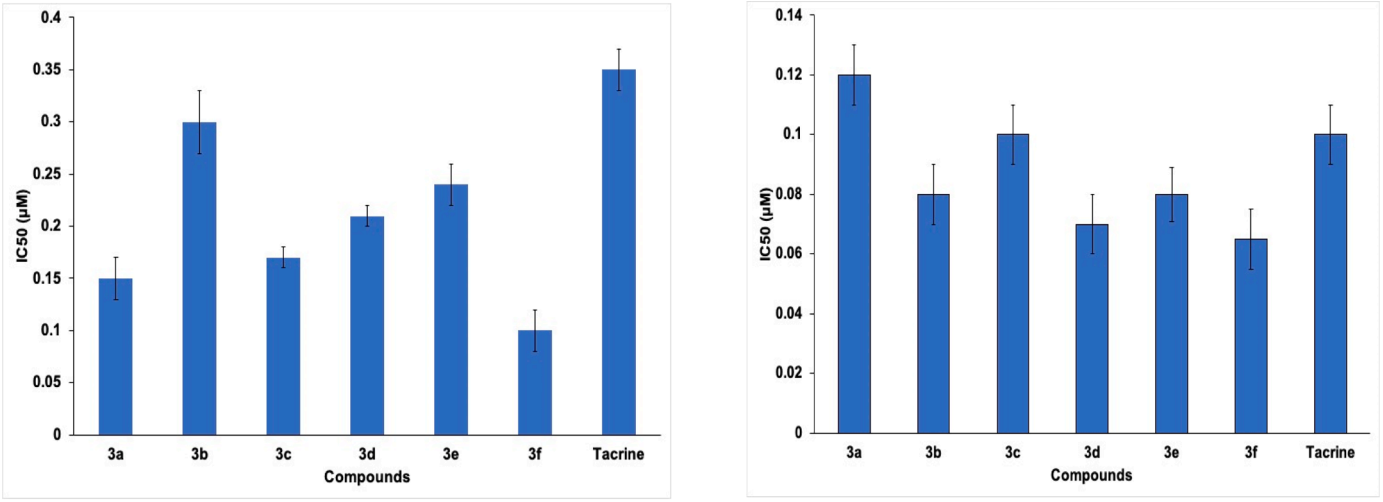

Fig. 6. The graphical presentation of IC_{50} values of synthesised molecules targeting (a) AChE and (b) BChE.

Table 3
The antioxidant activity outcomes of all Schiff base scaffolds.

Compound	DPPH Scavenging, IC_{50} (μM)
3a	478 ± 4
3b	658 ± 3
3c	763 ± 6
3d	587± 5
3e	687 ± 6
3f	354 ± 4
Tacrine	>1000

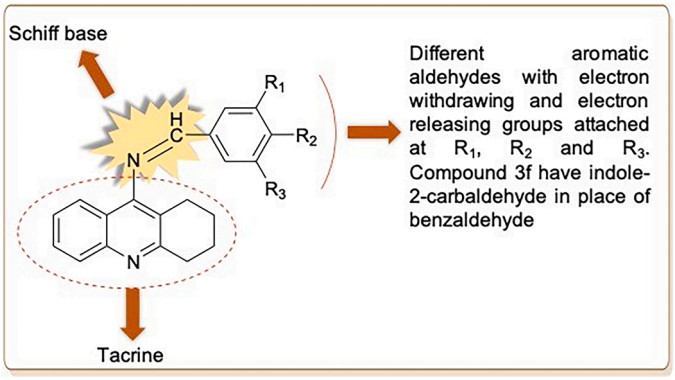

Fig. 7. Representation of Tacrine modified Schiff base scaffolds for SAR studies.

3.5. Pharmacokinetic predications

To evaluate the proposed compound ability to access targets in their bioactive form, pharmacokinetic tests were conducted using the SwissADME and pkCSM online platforms. In chemotherapeutic biochemical analyses, these methods accurately predicted outcomes [57]. The orally bioavailable state of six molecules, 3a–f, has been predicted. The developed compounds are BBB permeant, highly absorbable in the gastrointestinal tract, and contain P-glycoprotein (B3, B5, B6, B8, and B10), according to Table 5, which also shows the drug-likeness and ADMET features of the molecules. Due to their high HIA (>0.5 and >90 %, respectively) and optimal $CaCO_3$ cell permeability (>0.5), all drugs have excellent oral availability (Table 5). According to these findings, the molecules are mostly evenly distributed throughout plasma and

Table 4
The significant amino acid residues of active site interactions occurred during molecular docking along with the docking score.

Active Molecules	Interactions - Amino acid residues	Docking score (kcal/mol)
3f (AChE)	Hydrogen Bond - TYR124, TYR337, Vander Waal - SER203, HIS447, GLY123, TRP236, PHE297, VAL294, PHE295, PHE338, ASN87, ASP74. Pi-donor hydrogen bond - SER125 Pi-pi stacked - TYR341 Pi-alkyl – TRP86	−11.3
3f (BChE)	Hydrogen Bond – TRP82 Vander Waal – SER198, HIS438, THR120, ASN83, SER79, TRP430, GLY117 Pi-anion – ASP70 π- π T-shaped – TYR332, GLY116 Amide π-stacked – PHE329, TRP231 π-alkyl – ALA328, LEU285	−10.8

have a high percentage of unbound molecules, which enables them to effectively interact with their pharmacological targets. All substances appear to have good renal clearance and are not kidney's organic cation transporter 2 (OCT2) substrates, according to the anticipated total clearance values (Table 5), which indicate how well the body removes a medicine. The Lipinski rule for the ADMET analysis of the proposed compounds is displayed in Table 6. Lipinski's protocol was followed by every design, suggesting that the compounds possess drug-like characteristics and are orally accessible.

4. Discussion

In the fields of medicinal and green chemistry, the incorporation of environmentally friendly methods such as solvent-free synthesis is crucial for advancing sustainable drug development. Traditional synthetic processes often rely on the use of organic solvents, which are not only harmful to the environment but also pose significant health and safety risks, including toxicity and flammability. Additionally, the disposal of these solvents contributes to chemical waste, further exacerbating environmental pollution. By adopting solvent-free synthesis, we can effectively mitigate these risks, streamline chemical processes, and achieve cost savings by eliminating the need for expensive and hazardous solvents.

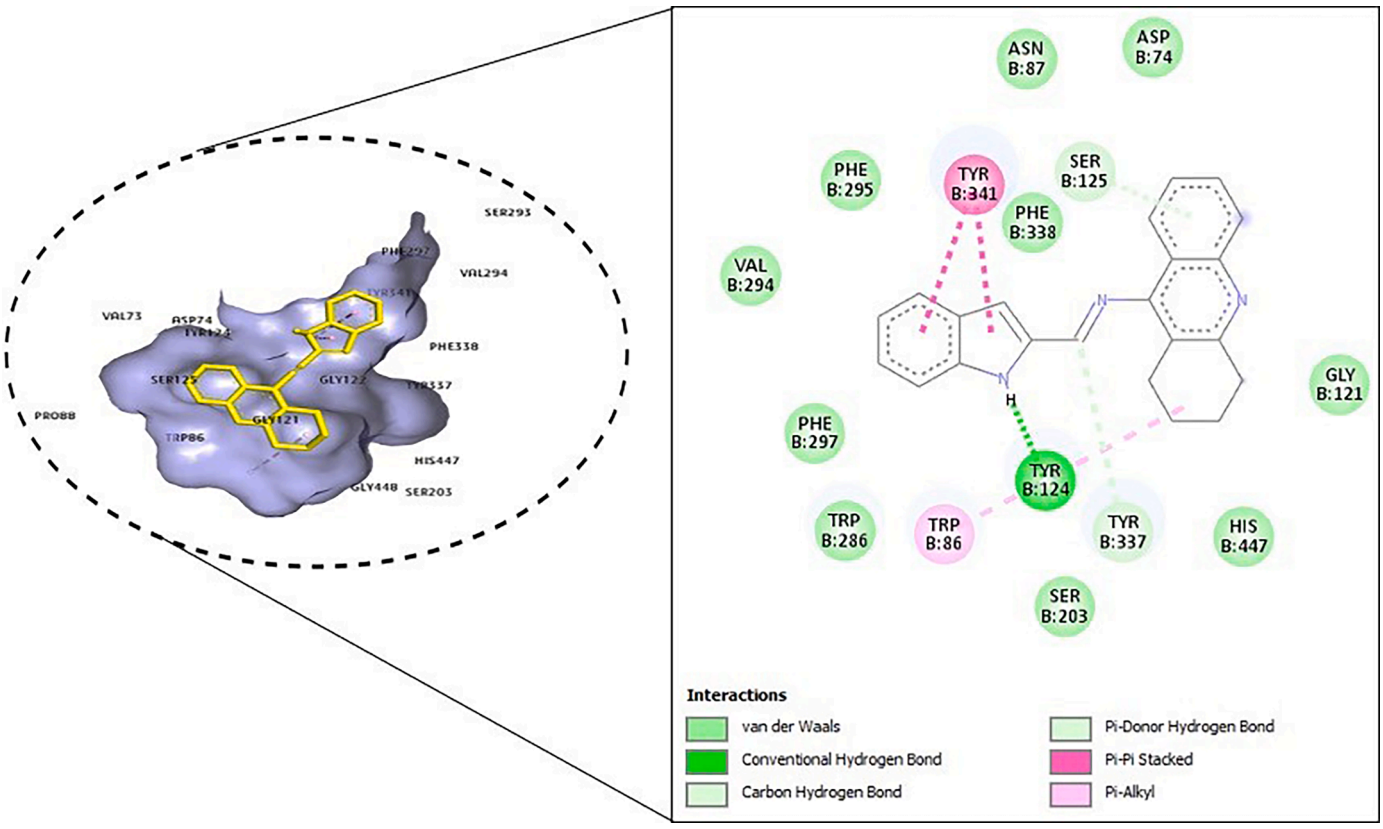

Fig. 8. The ligand-protein 2D and 3D interactions at enzymes catalytic site (AChE).

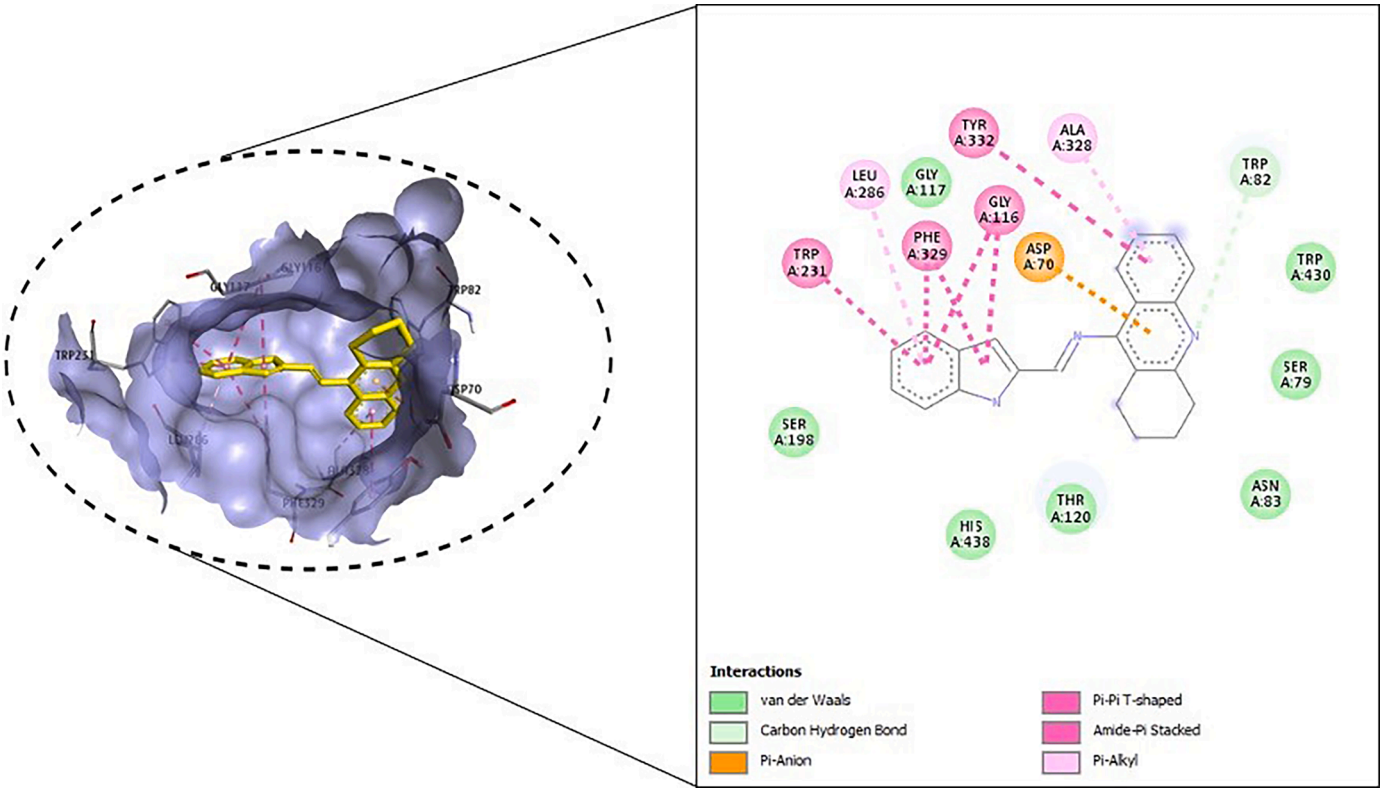

Fig. 9. The ligand-protein 2D and 3D interactions at enzymes catalytic site (BChE).

Table 5
Drug metabolism variables and the health effects of synthetic molecules.

Pharmacokinetic	Details	3a	3b	3c	3d	3e	3f
Absorption	(log Papp in 10^{-6} cm/s) $CaCo_3$	0.421	0.763	1.237	0.571	0.891	0.831
	Human Intestinal Absorption in %	90.128	90.752	92.541	90.586	90.782	90.873
	(log Kp)	−2.867	−2.849	−2.891	−2.861	−2.973	−2.652
	Skin permeability						
Distribution	(log L/kg)	0.076	0.0465	0.163	−0.023	0.042	0.031
	VD_{ss} (human)	0.141	0.127	0.122	0.1621	0.128	0.223
	Fraction unbound (human)	−0.413	−0.317	−0.236	−0.451	−0.426	−0.324
	(logBB)	−1.641	−1.687	−1.52	−1.654	−1.673	−1.973
	BBB permeability						
	(logPS)						
	CNS permeability						
Excretion	(log ml/min/kh)	0.121	0.113	0.235	0.110	0.103	0.211
	Total clearance	No	No	No	No	No	No
	Renal OCT2 substrate						
Toxicity	AMEX toxicity	2.764	2.761	0.251	0.167	0.156	0.127
	Oral rat acute toxicity (LD50)(mol kg^{-1})	−0.078	−0.062	2.83	2.824	2.765	2.881
	Minor toxicity (log mM)	0.431	−0.028	−0.451	−0.021	−0.017	−0.096

Table 6
Lipinski rule for ADMET analysis of synthesised compounds.

Compound	M.W	Rotatable bond	H-bond acceptors	H-bond donors	Log *P*	Solubility
3a	302.37	2	3	1	3.70	Moderately Soluble
3b	320.82	2	2	0	3.85	Soluble
3c	320.82	2	2	0	4.00	Soluble
3d	346.42	4	4	0	3.60	Soluble
3e	329.44	3	2	0	3.71	Soluble
3f	376.45	5	5	0	3.36	Soluble

In our research, we focused on the development of tacrine-modified Schiff base inhibitors as potential therapeutic agents for Alzheimer's disease. The synthesis of these compounds was carried out using a solvent-free grindstone method, a technique that involves the mechanical grinding of reactants to induce chemical reactions without the use of solvents. This approach is aligned with the principles of green chemistry, offering several advantages such as reduced energy consumption, minimal waste generation, and simplified reaction conditions. The grindstone technique is particularly well-suited for the formation of Schiff bases, where it facilitates the condensation of an aldehyde with a primary amine, leading to the desired product under mild and environmentally benign conditions.

To evaluate the biological efficacy of the synthesized Schiff base inhibitors, we employed a combination of in-silico molecular docking studies and in-vitro experiments. Molecular docking is a computational method used to predict the interaction between a ligand (in this case, the Schiff base inhibitors) and a biological target, such as the enzyme acetylcholinesterase (AChE), which plays a critical role in the pathogenesis of Alzheimer's disease [58]. The docking studies allowed us to model the binding of the tacrine-modified Schiff bases to the active site of AChE, providing insights into their potential as effective inhibitors. The results from the in-silico analysis were further validated through in-vitro experiments, where the binding affinity and inhibitory activity of the compounds were tested in a controlled laboratory setting. These complementary approaches not only confirmed the potential of the Schiff base inhibitors as therapeutic agents but also demonstrated the efficacy of combining green chemistry with modern computational and experimental techniques in drug development.

Our research contributes to the growing body of evidence supporting the integration of green chemistry principles in medicinal chemistry. The solvent-free synthesis of tacrine-modified Schiff base inhibitors, combined with in-silico and in-vitro validation, exemplifies a comprehensive approach to sustainable drug development. This research supports the United Nations Sustainable Development Goals.

Overall, this study highlights the potential of green chemistry to transform the field of medicinal chemistry, offering a path towards more sustainable and environmentally responsible drug development. By demonstrating the feasibility and benefits of solvent-free synthesis, our work paves the way for future research that prioritizes both therapeutic efficacy and environmental sustainability, ultimately contributing to the global effort to achieve a more sustainable and health-conscious society.

5. Conclusion

This research involved the design, synthesis, and evaluation of novel tacrine-modified Schiff base scaffolds for their cholinesterase inhibitory activity. The compounds exhibited varying degrees of inhibition against AChE and BChE, with compound 3f, featuring a heterocyclic ring, demonstrating the highest potency (IC50: 0.1 μM for AChE and 0.065 μM for BChE). Computational studies confirmed compound 3f as a potent inhibitor, displaying strong binding affinity at the active site of both enzymes. Additionally, these compounds showed superior antioxidant activity compared to tacrine, and ADMET predictions suggested favourable pharmacokinetic properties. The structure-activity relationship (SAR) analysis revealed that specific structural modifications, including heterocyclic groups and electron-donating or electron-withdrawing substituents, improved cholinesterase inhibition. These results highlight the potential of these derivatives as promising candidates for Alzheimer's treatment, with compound 3f standing out as a promising lead for further development.

CRediT authorship contribution statement

Presenjit: Visualization, Investigation, Writing – review & editing, Conceptualization. **Shubhra Chaturvedi:** Writing – review & editing, Supervision, Conceptualization. **Akanksha:** Writing – review & editing, Formal analysis. **Deepika Sharma:** Writing – review & editing. **Ritika Chaudhary:** Writing – review & editing, Validation. **Prachi Verma:** Writing – review & editing. **Ankita Singh:** Validation. **Kaman Singh:** Supervision.

Declaration of competing interest

The authors declare that they have no known competing financial interests or personal relationships that could have appeared to influence the work reported in this paper.

Acknowledgments

The authors would like to thank Department of Chemistry, Babasaheb Bhimrao Ambedkar University, Lucknow. Authors also gratefully acknowledge University Science Instrumentation Centre (USIC) for Instrumentation facility, University of Delhi, Delhi.

Supplementary materials

Supplementary material associated with this article can be found, in the online version, at doi:10.1016/j.chphi.2024.100759.

Data availability

Data will be made available on request.

References

[1] R. Jarosova, S.S. Niyangoda, P. Hettiarachchi, M.A. Johnson, Impaired dopamine release and latent learning in Alzheimer's disease model zebrafish, ACS Chem. Neurosci. 13 (2022) 2924–2931, https://doi.org/10.1021/acschemneuro.2c00484.
[2] A. Veluppal, Differentiation of Alzheimer conditions in brain MR images using bidimensional multiscale entropy-based texture analysis of lateral ventricles, Biomed. Signal Process Control 78 (2022) 103974, https://doi.org/10.1016/j.bspc.2022.103974.
[3] D.M. Skovronsky, V.M.Y. Lee, J.Q. Trojanowski, Neurodegenerative diseases: new concepts of pathogenesis and their therapeutic implications, Ann. Rev. Pathol.: Mechan. Dis. 1 (2006) 151–170, https://doi.org/10.1146/annurev.pathol.1.110304.100113.
[4] M. Pievani, W. de Haan, T. Wu, W.W. Seeley, G.B. Frisoni, Functional network disruption in the degenerative dementias, Lancet Neurol. 10 (2011) 829–843, https://doi.org/10.1016/S1474-4422(11)70158-2.
[5] R. Li, C. Zhang, Y. Rao, T.F. Yuan, Deep brain stimulation of fornix for memory improvement in alzheimer's disease: a critical review, Ageing Res. Rev. 79 (2022) 101668, https://doi.org/10.1016/j.arr.2022.101668.
[6] D. Osmaniye, I. Ahmad, B.N. Sağlık, S. Levent, H.M. Patel, Y. Ozkay, Z. A. Kaplancıklı, Design, synthesis, and molecular docking and ADME studies of novel hydrazone derivatives for AChE inhibitory, BBB permeability and antioxidant effects, J. Biomolecul. Struct. Dyn. (2022) 1–17, https://doi.org/10.1080/07391102.2022.2139762.
[7] H. Jindal, B. Bhatt, S. Sk, J. Singh Malik, Alzheimer disease immunotherapeutics: then and now, Hum. Vacc. Immunotherapeut. 10 (2014) 2741–2743, https://doi.org/10.4161/21645515.2014.970959.
[8] J. Hardy, N. Bogdanovic, B. Winblad, E. Portelius, N. Andreasen, A. Cedazo-Minguez, H. Zetterberg, Pathways to Alzheimer's disease, J. Intern. Med. 275 (2014) 296–303, https://doi.org/10.1111/joim.12192.
[9] M.S. Parihar, T. Hemnani, Alzheimer's disease pathogenesis and therapeutic interventions, J. Clin. Neurosci. 11 (2004) 456–467, https://doi.org/10.1016/j.jocn.2003.12.007.
[10] L. Parnetti, F. Mignini, D. Tomassoni, E. Traini, F. Amenta, Cholinergic precursors in the treatment of cognitive impairment of vascular origin: ineffective approaches or need for re- evaluation? J. Neurol. Sci. 257 (2007) 264–269, https://doi.org/10.1016/j.jns.2007.01.043.
[11] E. Başaran, R. Çakmak, M. Şentürk, T. Taskin-Tok, Biological activity and molecular docking studies of some N-phenylsulfonamides against cholinesterases and carbonic anhydrase isoenzymes, J. Molecul. Recognit. 35 (2022) e2982.
[12] L.A. Craig, N.S. Hong, R.J. McDonald, Revisiting the cholinergic hypothesis in the development of Alzheimer's disease, Neurosci. Biobehav. Rev. 35 (2011) 1397–1409, https://doi.org/10.1016/j.neubiorev.2011.03.001.
[13] J.L. Cummings, C. Back, The cholinergic hypothesis of neuropsychiatric symptoms in Alzheimer's disease, Am. J. Geriatr. Psychiatry 6 (1998) S64–S78, https://doi.org/10.1097/00019442-199821001-00009.
[14] M. Rusanen, M. Kivipelto, C.P. Quesenberry Jr, J. Zhou, R.A. Whitmer, Heavy smoking in midlife and long-term risk of Alzheimer disease and vascular dementia, Arch. Intern. Med. 171 (2011) 333–339, https://doi.org/10.1001/archinternmed.2010.393.
[15] R.J. Van Marum, Current and future therapy in Alzheimer's disease, Fundam. Clin. Pharmacol. 22 (3) (2008) 265–274, https://doi.org/10.1111/j.1472-8206.2008.00578.x.
[16] D.G. Wilkinson, P.T. Francis, E. Schwam, J. Payne-Parrish, Cholinesterase inhibitors used in the treatment of Alzheimer's disease, Drug. Aging 21 (2004) 453–478, https://doi.org/10.2165/00002512-200421070-00004.
[17] G.R. Dawson, S.D. Iversen, The effects of novel cholinesterase inhibitors and selective muscarinic receptor agonists in tests of reference and working memory, Behav. Brain Res. 57 (1993) 143–153, https://doi.org/10.1016/0166-4328(93)90130-I.
[18] J. Grutzendler, J.C. Morris, Cholinesterase inhibitors for Alzheimer's disease, Drugs 61 (2001) 41–52, https://doi.org/10.2165/00003495-200161010-00005.
[19] J.P. Teixeira, A.A. de Castro, F.V. Soares, E.F. da Cunha, T.C. Ramalho, Future therapeutic perspectives into the Alzheimer's disease targeting the oxidative stress hypothesis, Molecules 24 (2019) 4410, https://doi.org/10.3390/molecules24234410.
[20] W.R. Markesbery, Oxidative stress hypothesis in Alzheimer's disease, Free Rad. Biol. Med. 23 (1997) 134–147, https://doi.org/10.1016/S0891-5849(96)00629-6.
[21] C. Leeuwenburgh, J.W. Heinecke, Oxidative stress and antioxidants in exercise, Curr. Med. Chem. 8 (2001) 829–838, https://doi.org/10.2174/0929867013372896.
[22] A.V. Rao, B. Balachandran, Role of oxidative stress and antioxidants in neurodegenerative diseases, Nutr. Neurosci. 5 (2002) 291–309, https://doi.org/10.1080/1028415021000033767.
[23] M. Shidore, J. Machhi, K. Shingala, P. Murumkar, M.K. Sharma, N. Agrawal, A. Tripathi, Z. Parikh, P. Pillai, M.R. Yadav, Benzylpiperidine-linked diarylthiazoles as potential anti-Alzheimer's agents: synthesis and biological evaluation, J. Med. Chem. 59 (12) (2016) 5823–5846.
[24] R Ulus,B.ZenginKurt, I Gaziog˘lu,M.Kaya, Microwaveassistedsynthesisofnovel hybrid tacrine-sulfonamide derivatives and investigation of their antioxidant and anticholinesterase activities, Bioorg. Chem. 70 (2017) 245–255.
[25] Z.-P. Wu, X.-W. Wu, T. Shen, Y.-P. Li, X.i. Cheng, L.-Q. Gu, Z.-S. Huang, L.-K. An, Synthesis and acetylcholinesterase and butyrylcholinesterase inhibitory activities of 7-alkoxyl substituted indolizinoquinoline-5,12-dione derivatives, Arch. Pharm. (Weinheim) 345 (3) (2012) 175–184.
[26] B.N. Sag˘lık, S. Ilgın, Y.O. ̈zkay, Synthesis of new donepezil analogues and investigation of their effects on cholinesterase enzymes, Eur. J. Med. Chem. 124 (2016) 1026–1040.
[27] B.Z. Kurt, I. Gazioglu, A. Dag, R.E. Salmas, G. Kayık, S. Durdagi, F. Sonmez, Synthesis, anticholinesterase activity and molecular modeling study of novel carbamate-substituted thymol/carvacrol derivatives, Bioorgan. Med. Chem. 25 (4) (2017) 1352–1363.
[28] Z. Chen, M. Digiacomo, Y. Tu, Q. Gu, S. Wang, X. Yang, J. Chu, Q. Chen, Y. Han, J. Chen, G. Nesi, S. Sestito, M. Macchia, S. Rapposelli, R. Pi, Discovery of novel rivastigmine-hydroxycinnamic acid hybrids as multi-targeted agents for Alzheimer's disease, Eur. J. Med. Chem. 125 (2017) 784–792.
[29] S. Onur, et al., Synthesis, characterization and antibacterial effect of diarylmethylamine-based imines, J. Mol. Struct. (2020) 1214.
[30] S. Onur, et al., New imino-methoxy derivatives: design, synthesis, characterization, antimicrobial activity, DNA interaction and molecular docking studies, J. Biomol. Struct. Dyn. 0 (2021) 1–13.
[31] S. Afrin Dalia, et al., A short review on chemistry of schiff base metal complexes and their catalytic application, ~ 2859.Int, J. Chem. Stud. 6 (2018) 2859–2866.
[32] G. Orhan, İ. Orhan, N. Subutay-Öztekin, F. Ak, B. Şener, Contemporary anticholinesterase pharmaceuticals of natural origin and their synthetic analogues for the treatment of Alzheimer's disease, Recent Pat CNS Drug Discov. 4 (2009) 43–51.
[33] W.K. Summers, L.V. Majovski, G.M. Marsh, K. Tachiki, A. Kling, Oral tetrahydroaminoacridine in long- term treatment of senile dementia, Alzheimer type, New Engl. J. Med. 315 (1986) 1241–1245.
[34] M. Harel, I. Schalk, L. Ehret-Sabatier, F. Bouet, M. Goeldner, C. Hirth, P.H. Axelsen, I. Silman, J.L. Sussman, Quaternary ligand binding to aromatic residues in the active-site gorge of acetylcholinesterase, Proc. Natl. Acad. Sci. 90 (19) (1993) 9031–9035.
[35] H. Khalid, A.U. Rehman, M.A. Abbasi, R. Hussain, K.M. Khan, M. Ashraf, S.A. Ejaz, M.Q. Fatmi, Synthesis, biological evaluation, and molecular docking of N'- (Aryl/alkylsulfonyl)-1-(phenylsulfonyl) piperidine-4- carbohydrazide derivatives, Turk. J. Chem 38 (2014) 189–201.
[36] A. Dişli, M. Gümüş, K. Ünal, N. Sarı, F. Arslan, New multifunctional agents and their inhibitory effects on the acetyl cholinesterase enzyme, Maced. J. Chem. Chem. Eng. 37 (1) (2018) 21–34.
[37] İ. Şakıyan, E.A. Koyuncu, F. Arslan, H. Öğütçü, N. Sarı, Some novel antimicrobial therapeutic agents for acetylcholinesterase inhibitors; synthesis of hydroxy-quinoline ester involving amino acid, G. U, J. Sci. 28 (1) (2015) 11–19.
[38] D. Schuster, M. Spetea, M. Music, S. Rief, M. Fink, J. Kirchmair, J. Schütz, G. Wolber, T. Langer, H. Stuppner, et al., Morphinans and isoquinolines: acetylcholinesterase inhibition, pharmacophore modeling, and interaction with opioid receptors, Bioorg. Med. Chem. 18 (2010) 5071–5080.
[39] S. Yılmaz, Y. Akbaba, B. Özgeriş, L.P. Köse, S. Göksu, İ. Gülçin, S.H. Alwasel, C. T. Supuran, Synthesis and inhibitory properties of some carbamates on carbonic anhydrase and acetylcholine esterase, J. Enzyme Inhib. Med. Chem., Early Online (2016) 1–8.
[40] B. Turan, K. Şendil, E. Şengül, M.S. Gültekin, P. Taslimi, İ. Gulçin, C.T. Supuran, The synthesis of some β-lactams and investigation of their metal-chelating activity, carbonic anhydrase and acetylcholinesterase inhibition profiles, J. Enzyme Inhib. Med. Chem. Early Online (2016) 1–10.
[41] S. Singla, P. Piplani, Coumarin derivatives as potential inhibitors of acetylcholinesterase: synthesis, molecular docking and biological studies, Bioorg. Med. Chem. 24 (2016) 4587–4599.
[42] M. Benchekroun, M. Bartolini, J. Egea, A. Romero, E. Soriano, M. Pudlo, V. Luzet, V. Andrisano, M.N. Jimeno, M.G. Lopéz, et al., Novel tacrine-grafted ugi adducts as

multipotent anti-Alzheimer drugs: a synthetic renewal in tacrine-ferulic acid hybrids, ChemMedChem 10 (3) (2015) 523–539.
[43] M. Rosini, E. Simoni, M. Bartolini, A. Tarozzi, R. Matera, A. Milelli, Exploiting the lipoic acid structure in the search for novel multitarget ligands against Alzheimer's disease, Eur. J. Med. Chem. 46 (2011) 5435–5442.
[44] Z. Liu, L. Fang, H. Zhang, S. Gou, L. Chen, Design, synthesis and biological evaluation of multifunctional tacrine-curcumin hybrids as new cholinesterase inhibitors with metal ions-chelating and neuroprotective property, Bioorg. Med. Chem. 25 (2017) 2387–2398.
[45] H.H. Afridi, M. Shoaib, F.A. Al-Joufi, S.W.A. Shah, H. Hussain, A. Ullah, E. U. Mughal, Synthesis and investigation of the analgesic potential of enantiomerically pure schiff bases: a mechanistic approach, Molecules 27 (16) (2022) 5206.
[46] G.L. Ellman, K.D. Courtney, V. Andres Jr, R.M. Featherstone, A new and rapid colorimetric determination of acetylcholinesterase activity, Biochem. Pharmacol. 7 (1961) 88–90, https://doi.org/10.1016/0006-2952(61)90145-9.
[47] R. Çakmak, E. Çınar, E. Başaran, M. Boğa, Synthesis, characterization and biological evaluation of ester derivatives of 4-(diethylamino) salicylaldehyde as cholinesterase, and tyrosinase inhibitors, Middle East J. Sci. 7 (2021) 137–144, https://doi.org/10.51477/mejs.947973.
[48] M.S. Blois, Antioxidant determinations by the use of a stable free radical, Nature 181 (1958) 1199–1200, https://doi.org/10.1038/1811199a0.
[49] R. Çakmak, E. Başaran, M. Boğa, Ö. Erdoğan, E. Çınar, Ö. Çevik, Schiff base derivatives of 4-aminoantipyrine as promising molecules: synthesis, structural characterization, and biological activities, Russ. J. Bioorgan. Chem. 48 (2022) 334–344, https://doi.org/10.1134/S1068162022020182.
[50] A. Daina, O. Michielin, V. Zoete, SwissADME: A free web tool to evaluate pharmacokinetics, drug-likeness and medicinal chemistry friendliness of small molecules, Sci. Rep. 7 (1) (2017) 42717.
[51] D. Biovia, H. Berman, J. Westbrook, Z. Feng, G. Gilliland, T. Bhat, "Discovery studio visualizer," 17.2, Dassault Systèmes BIOVIA.
[52] W. Tian, C. Chen, X. Lei, J. Zhao, J. Liang, CASTp: computed Atlas of Surface Topography of proteins, Nucl. Acid. Res. (2018).
[53] J. Eberhardt, D. Santos-Martins, AutoDock Vina 1.2.0: new docking methods, expanded force field, NCBI (2023).
[54] X.Y. Zhang, H.J. Huang, D.L. Zhuang, M.I. Nasser, M.H. Yang, P. Zhu, M.Y. Zhao, Biological, clinical and epidemiological features of COVID-19, SARS and MERS and AutoDock simulation of ACE2, Infect. Dis. Pov. 9 (04) (2020) 10–20.
[55] D. Dey, R. Hossain, P. Biswas, P. Paul, M.A. Islam, T.I. Ema, B. Kim, Amentoflavone derivatives significantly act towards the main protease (3CLPRO/MPRO) of SARS-CoV-2: in silico admet profiling, molecular docking, molecular dynamics simulation, network pharmacology, Mol. Divers. 27 (2) (2023) 857–871.
[56] Presenjit, S. Chaturvedi, A. Singh, D. Gautam, K. Singh, A.K. Mishra, An insight into the Effect of Schiff Base and their d and f Block Metal complexes on various Cancer cell lines as Anticancer agents: a review, Anticancer Agents Med. Chem. 24 (7) (2024) 488–503.
[57] M.K. Matlock, T.B. Hughes, J.L. Dahlin, S.J. Swamidass, J. Chem. Inf. Model. 58 (2018) 1483–1500.
[58] A. Sharma, A. Yadav, K. Cwiklinski, E. Quaye, R. Aalinkeel, S.D. Mahajan, R. K. Sharma, In-vitro studies of curcumin encapsulated mesoporous Fe-Phenanthroline nanocluster for reduction of amyloid β plaque, J. Drug. Deliv. Sci. Technol. 54 (2019) 101314.